

[Click here to view linked References](#)

1 **Electrochemical destruction of *trans*-cinnamic acid by**  
2  
3  
4 **advanced oxidation processes: Kinetics, mineralization and**  
5  
6  
7  
8 **degradation route**  
9

10  
11  
12 Nelly Flores, Abdoulaye Thiam, Rosa María Rodríguez, Francesc Centellas, Pere

13  
14  
15 Lluís Cabot, José Antonio Garrido, Enric Brillas\*, Ignasi Sirés

16  
17  
18 *Laboratori d'Electroquímica dels Materials i del Medi Ambient, Departament de Química Física,*

19  
20  
21 *Facultat de Química, Universitat de Barcelona, Martí i Franquès 1-11, 08028 Barcelona, Spain*  
22  
23  
24  
25  
26  
27  
28  
29  
30  
31  
32  
33  
34  
35  
36  
37

38 Article submitted for publication in *Environmental Science and Pollution Research*  
39  
40  
41  
42  
43  
44  
45  
46  
47  
48  
49  
50  
51  
52  
53  
54  
55  
56

57 \* Corresponding author: Tel.: +34 934021223; fax: +34 934021231  
58

59 *E-mail address:* brillas@ub.edu (E. Brillas)  
60  
61  
62  
63  
64  
65

1  
2  
3  
4  
5  
6  
7  
8  
9  
10  
11  
12  
13  
14  
15  
16  
17  
18  
19  
20  
21  
22  
23  
24  
25  
26  
27  
28  
29  
30  
31  
32  
33  
34  
35  
36  
37  
38  
39  
40  
41  
42  
43  
44  
45  
46  
47  
48  
49  
50  
51  
52  
53  
54  
55  
56  
57  
58  
59  
60  
61  
62  
63  
64  
65

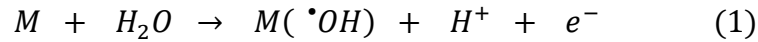
**Abstract** Acidic solutions of *trans*-cinnamic acid at pH 3.0 have been comparatively treated by anodic oxidation with electrogenerated H<sub>2</sub>O<sub>2</sub> (AO-H<sub>2</sub>O<sub>2</sub>), electro-Fenton (EF) and photoelectro-Fenton (PEF). The electrolytic experiments were carried out with a boron-doped diamond (BDD)/air-diffusion cell. The substrate was very slowly abated by AO-H<sub>2</sub>O<sub>2</sub> because of its low reaction rate with oxidizing •OH produced from water discharge at the BDD anode. In contrast, its removal was very rapid and at similar rate by EF and PEF due to the additional oxidation by •OH in the bulk, formed from Fenton's reaction between cathodically generated H<sub>2</sub>O<sub>2</sub> and added Fe<sup>2+</sup>. The AO-H<sub>2</sub>O<sub>2</sub> treatment yielded the lowest mineralization. The EF process led to persistent final products like Fe(III) complexes, which were quickly photolyzed upon UVA irradiation in PEF to give an almost total mineralization with 98% total organic carbon removal. The effect of current density and substrate concentration on all the mineralization processes was examined. GC-MS analysis of electrolyzed solutions allowed identifying five primary aromatics and one heteroaromatic molecule, whereas final carboxylic acids like fumaric, acetic and oxalic were quantified by ion-exclusion HPLC. From all the products detected, a degradation route for *trans*-cinnamic acid is proposed.

*Keywords:* Anodic oxidation; Electro-Fenton; Hydroxyl radical; Oxidation products; Photoelectro-Fenton; Photolysis; *trans*-Cinnamic acid; Water treatment

## Introduction

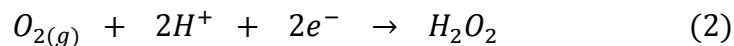
*trans*-Cinnamic acid (*E*-3-phenyl-2-propenoic acid) is an unsaturated carboxylic acid commonly present in many fruits and vegetables. It is obtained from oil of cinnamon, balsams such as storax and shea butter, and it is synthesized in the industry from the base-catalyzed condensation of acetic anhydride and benzaldehyde or from reaction between cinnamaldehyde and benzal chloride. It is largely used worldwide in fragrances including decorative cosmetics, fine fragrances, shampoos, toilet soaps and other toiletries as well as in non-cosmetic products such as household cleaners and detergents (Letizia et al. 2005). *trans*-Cinnamic acid has antifungal properties, inhibits the toxicity of metals in plants (Hojati et al. 2015) and acts as an antioxidant with very low toxicity in bacteria, animals and human beings (Letizia et al. 2005; Zeni et al. 2013; Hakkim et al. 2014). It is a main component of toxic and recalcitrant olive oil mill wastewater (OOMWW), where its concentration reaches up to 106 mg L<sup>-1</sup> (Deeb et al. 2012), and it has been detected at relatively high contents of 10 µg L<sup>-1</sup> in rivers (Lafont et al. 2001). Kontos et al. (2014) described the removal and recovery of *trans*-cinnamic acid from OOMWW by crystallization. Several authors have reported the degradation of this acid and some polyphenolic components of OOMWW using different bacteria strains (Di Gioia et al. 2012) and by several advanced oxidation processes (AOPs) including zero-valent iron (Sanchez et al. 2012) and wet oxidation (Lopes et al. 2007; Lopes and Quinta-Ferreira 2010). AOPs are based on the oxidation of pollutants by in situ generated reactive oxygen species (ROS) like hydroxyl radical ( $\bullet\text{OH}$ ). However, much less is known about the treatment of *trans*-cinnamic acid solutions by powerful electrochemical AOPs (EAOPs). Chatzisyneon et al. (2009) found a very poor mineralization with 25% chemical oxygen demand (COD) reduction upon anodic oxidation (AO) treatment of 110 mL of a 5 mM *trans*-cinnamic acid solution in 0.1 M HClO<sub>4</sub> using a Ti/IrO<sub>2</sub> anode after a specific charge consumption of 28 Ah L<sup>-1</sup>. These authors also describe a similar COD abatement of 30% for OOMWW with 5 mM NaCl after consuming 43 Ah L<sup>-1</sup>.

1  
2  
3  
4  
5  
6  
7  
8  
9  
10  
11  
12  
13  
14  
15  
16  
17  
18  
19  
20  
21  
22  
23  
24  
25  
26  
27  
28  
29  
30  
AO is the most popular EAOP and consists in the application of a high current density ( $j$ ) to the anode M of the cell for the direct anodic oxidation of pollutants or, primordially, for their destruction by physisorbed hydroxyl radical  $M(\bullet OH)$  produced as intermediate of water discharge to  $O_2$  at the anode surface (Marselli et al. 2003; Martínez-Huitle and Ferro 2006; Panizza and Cerisola 2009; Brillas and Martínez-Huitle 2015):

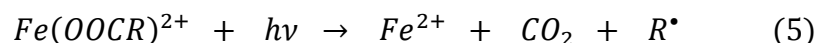
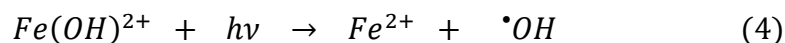
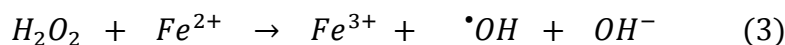


16  
17  
18  
19  
20  
21  
22  
23  
24  
25  
26  
27  
28  
29  
30  
31  
32  
33  
34  
35  
36  
37  
38  
39  
40  
41  
42  
43  
44  
45  
46  
47  
48  
49  
50  
51  
52  
53  
54  
55  
56  
57  
58  
59  
60  
61  
62  
63  
64  
65  
AO is more effective when a boron-doped diamond (BDD) thin-film electrode is employed as anode. This is due to the higher oxidation ability of physisorbed BDD( $\bullet OH$ ) generated by reaction (1) compared to that of other physisorbed  $M(\bullet OH)$  produced at anodes like Pt and  $PbO_2$  (Ciríaco et al. 2009; Guinea et al. 2009; Rodrigo et al. 2010; Cavalcanti et al. 2013), as a result of the low interaction BDD- $\bullet OH$  and the larger  $O_2$ -overpotential of BDD that favors the reaction of  $\bullet OH$  with organics (Panizza and Cerisola 2009).

31  
32  
33  
34  
35  
36  
37  
38  
39  
40  
41  
42  
43  
44  
45  
46  
47  
48  
49  
50  
51  
52  
53  
54  
55  
56  
57  
58  
59  
60  
61  
62  
63  
64  
65  
The oxidation ability of AO with a BDD anode can be enhanced in an undivided cell by electrogenerating  $H_2O_2$  at the cathode from the two-electron reduction of  $O_2$  gas via reaction (2). The so-called AO- $H_2O_2$  process involves the destruction of organics preferentially by physisorbed BDD( $\bullet OH$ ), with only a minor participation of ROS like  $H_2O_2$  and its anodic oxidation product  $HO_2\bullet$  (Sirés and Brillas 2012; Sirés et al. 2014). Carbon nanotubes (Khataee et al. 2013, 2014), graphite felt (Vatanpour et al. 2009), activated carbon fiber (Wang et al. 2008), carbon modified with metals or metal oxide nanoparticles (Assumpção et al. 2013), carbon felt (Dirany et al. 2012; El-Ghenymy et al. 2014; Yahya et al. 2014), carbon-polytetrafluoroethylene (PTFE)  $O_2$  or air-diffusion (Borràs et al. 2010; Thiam et al. 2014, 2015b) and BDD (Cruz-González et al. 2010, 2012) are considered the most suitable carbonaceous cathodes to electrogenerate  $H_2O_2$ .



The performance of AO-H<sub>2</sub>O<sub>2</sub> can be improved by means of EAOPs based on Fenton's reaction chemistry like electro-Fenton (EF) and photoelectro-Fenton (PEF), which have recently gained increasing interest for wastewater remediation (Sirés and Brillas 2012; Sirés et al. 2014; Vasudevan and Oturan 2014; Brillas and Martínez-Huitle 2015). In the EF process, a small quantity of Fe<sup>2+</sup> is added to the solution to react with H<sub>2</sub>O<sub>2</sub> via Fenton's reaction (3) yielding Fe<sup>3+</sup> and •OH in the bulk (Dirany et al. 2012; El-Ghenymy et al. 2014; Thiam et al. 2014, 2015a). Organics are then destroyed by both radicals, M(•OH) and •OH, at an optimum pH ~ 3. When the PEF process is applied, the treated solution is irradiated with artificial UVA light that causes the photoreduction of Fe(OH)<sup>2+</sup> species to Fe<sup>2+</sup> and •OH generation via reaction (4), along with the photodecarboxylation of complexes of Fe(III) with generated carboxylic acids from reaction (5) (Ruiz et al. 2011; Moreira et al. 2013; Florenza et al. 2014; Thiam et al. 2015a).



In this paper, we present a comparative study on the degradation of *trans*-cinnamic acid solutions of pH 3.0 by AO-H<sub>2</sub>O<sub>2</sub>, EF and PEF using a stirred BDD/air-diffusion cell. The influence of *j* and substrate content on the performance of these EAOPs was examined to clarify the role of generated hydroxyl radicals and UV light. The abatement of *trans*-cinnamic acid and the evolution of final carboxylic acids were followed by high-performance liquid chromatography (HPLC). Gas chromatography-mass spectrometry (GC-MS) allowed the identification of the primary aromatic intermediates. A plausible route for *trans*-cinnamic acid mineralization including all detected products is proposed.

## Experimental details

### Chemicals

Analytical grade *trans*-cinnamic acid (purity > 99%) was supplied by Sigma-Aldrich and used as received. Acetic, fumaric and oxalic acids were of analytical grade purchased from Panreac. Heptahydrated Fe(II) sulfate and anhydrous sodium sulfate were of analytical grade supplied by Fluka. Analytical grade sulfuric acid was purchased from Merck and used to adjust the initial solution pH to 3.0. The solutions were prepared with ultrapure water provided by a Millipore Milli-Q system (resistivity > 18.2 MΩ cm at 25 °C). Other chemicals were of HPLC or analytical grade supplied by Avocado, Fluka and Merck.

### Electrolytic system

The electrolytic assays were carried out in an open and undivided cylindrical glass cell of 150 mL capacity equipped with a double jacket for recirculating water through a Thermo Electron Corporation HAAKE DC 10 thermostat. All the experiments were made at 25 °C and under vigorous stirring with a magnetic bar at 700 rpm to ensure the solution mixing and the transport of reactants toward/from the electrodes. A 3 cm<sup>2</sup> BDD thin-film electrode from NeoCoat (La-Chaux-de-Fonds, Switzerland) was used as the anode and a 3 cm<sup>2</sup> carbon-PTFE air-diffusion cathode from E-TEK (Somerset, NJ, USA) was used as the cathode. The air-diffusion cathode was mounted as described elsewhere (Boye et al. 2003) and was fed with air pumped at 300 mL min<sup>-1</sup> for H<sub>2</sub>O<sub>2</sub> generation. The interelectrode gap was about 1 cm. The trials were performed at constant *j* provided by an EG&G Princeton Applied Research 273A potentiostat-galvanostat.

Comparative treatment of 100 mL of solutions with *trans*-cinnamic acid and 0.05 M Na<sub>2</sub>SO<sub>4</sub> as background electrolyte at pH 3.0 was carried out by AO-H<sub>2</sub>O<sub>2</sub>, EF and PEF. Electrolyses for the two latter EAOPs were run after addition of 0.50 mM Fe<sup>2+</sup> as catalyst since this content was found optimal for many organics treated under similar conditions (Ruiz et al. 2011; Moreira et al. 2013;

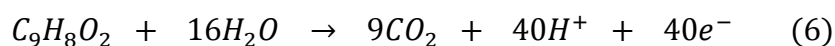
1  
2  
3  
4  
5  
6  
7  
8  
9  
10  
11  
12  
13  
14  
15  
16  
17  
18  
19  
20  
21  
22  
23  
24  
25  
26  
27  
28  
29  
30  
31  
32  
33  
34  
35  
36  
37  
38  
39  
40  
41  
42  
43  
44  
45  
46  
47  
48  
49  
50  
51  
52  
53  
54  
55  
56  
57  
58  
59  
60  
61  
62  
63  
64  
65

Florenza et al. 2014; Thiam et al. 2015a). For PEF, a Philips TL/6W/08 fluorescent black light blue tube was placed at 8 cm above the solution. This UVA lamp emitted at  $\lambda_{\max} = 360$  nm and with 5 W  $\text{m}^{-2}$  average power density, as determined with a Kipp&Zonen CUV 5 UV radiometer.

## Instruments and analytical procedures

A Crison GLP 22 pH-meter was used to measure the solution pH. Total organic carbon (TOC) was determined with a Shimadzu VCSN TOC analyzer. This analysis was performed by filtering the samples withdrawn from treated solutions at regular times with Whatman 0.45  $\mu\text{m}$  PTFE filters and, subsequently, directly injecting 50  $\mu\text{L}$  aliquots into the above analyzer. Reproducible TOC values with  $\pm 1\%$  accuracy were always determined.

Since the total conversion of *trans*-cinnamic acid into  $\text{CO}_2$  can be written as follows:



the mineralization current efficiency (MCE) for each trial was then estimated from Eq. (7) (Ruiz et al. 2011):

$$\text{MCE}(\%) = \frac{nFV\Delta(\text{TOC})_{\text{exp}}}{4.32 \times 10^7 \text{mlt}} \times 100 \quad (7)$$

where  $n$  is the number of electrons for total mineralization (40  $\text{e}^-$  from reaction (6)),  $F$  is the Faraday constant (96,487  $\text{C mol}^{-1}$ ),  $V$  is the solution volume (in L),  $\Delta(\text{TOC})_{\text{exp}}$  is the experimental TOC abatement (in  $\text{mg L}^{-1}$ ),  $4.32 \times 10^7$  is a conversion factor ( $3,600 \text{ s h}^{-1} \times 12,000 \text{ mg C mol}^{-1}$ ),  $m$  is the number of carbon atoms of *trans*-cinnamic acid (9 C atoms),  $I$  is the current (in A) and  $t$  is the electrolysis time (in h).

Reversed-phase HPLC was used to follow the kinetic decay of *trans*-cinnamic acid. These measurements were made by injecting 10  $\mu\text{L}$  aliquots into a Waters 600 LC containing a BDS Hypersil C18 6  $\mu\text{m}$ , 250 mm  $\times$  4.6 mm, column at 35  $^\circ\text{C}$ , coupled to a Waters 996 photodiode array detector selected at  $\lambda = 276$  nm. All the samples were filtered with Whatman 0.45  $\mu\text{m}$

1 PTFE filters, although for the EF and PEF assays, they were previously diluted with acetonitrile  
2 (1:1) to stop the degradation process. The mobile phase was an 80:20 (v/v) acetonitrile/water  
3  
4 mixture eluted at 0.8 mL min<sup>-1</sup> and the chromatograms exhibited a well-defined peak for *trans*-  
5  
6 cinnamic acid at retention time ( $t_r$ ) = 3.45 min.  
7  
8

9 The same LC system was used to detect and quantify the generated carboxylic acids by ion-  
10  
11 exclusion HPLC, but with a Bio-Rad Aminex HPX 87H, 300 mm × 7.8 mm, column at 35 °C  
12  
13 and the photodiode array detector set at  $\lambda = 210$  nm. This analysis was also performed with 10  
14  
15  $\mu$ L aliquots, circulating 4 mM H<sub>2</sub>SO<sub>4</sub> at 0.6 mL min<sup>-1</sup> as mobile phase. The chromatograms  
16  
17 recorded displayed peaks associated to oxalic ( $t_r = 6.9$  min), acetic ( $t_r = 14.9$  min) and fumaric  
18  
19 ( $t_r = 15.6$  min) acids.  
20  
21  
22  
23

24 The primary aromatic products of *trans*-cinnamic acid were identified from the AO-H<sub>2</sub>O<sub>2</sub>  
25  
26 treatment of 100 mL of a 0.926 mM substrate solution at 33.3 mA cm<sup>-2</sup>. Various electrolyses were  
27  
28 run up to 30 and 90 min and the remaining organic components of each solution were extracted out  
29  
30 with CH<sub>2</sub>Cl<sub>2</sub> (3 × 25 mL). The resulting organic fractions were dried over anhydrous Na<sub>2</sub>SO<sub>4</sub>,  
31  
32 filtered and their volume reduced to near 1 mL for further analysis by GC-MS using a NIST05-MS  
33  
34 library to elucidate the mass spectra. GC-MS measurements were performed with an Agilent  
35  
36 Technologies system composed of a 6890N GC and a 5975C MS operating in electron impact mode  
37  
38 at 70 eV. The GC was fitted with either a non-polar Agilent J&W HP-5ms or a polar HP INNOWax  
39  
40 column, both of 0.25  $\mu$ m, 30 m × 0.25 mm. The temperature ramp was: 36 °C for 1 min, 5 °C min<sup>-1</sup>  
41  
42 up to 300 °C for the non-polar column or 250 °C for the polar one, and hold time 10 min. The  
43  
44 temperature of the inlet, source and transfer line was 250, 230 and 280 °C for the non-polar column  
45  
46 and 250, 230 and 250 °C for the polar one.  
47  
48  
49  
50  
51  
52  
53  
54  
55  
56  
57  
58  
59  
60  
61  
62  
63  
64  
65



## Results and discussion

### Kinetic decay of *trans*-cinnamic acid by AO-H<sub>2</sub>O<sub>2</sub>, EF and PEF

The decay kinetics of *trans*-cinnamic acid by the different EAOPs using a BDD/air-diffusion cell was first determined for 100 mL of 0.926 mM substrate solutions in 0.05 M Na<sub>2</sub>SO<sub>4</sub> of pH 3.0 at 33.3 mA cm<sup>-2</sup>. In AO-H<sub>2</sub>O<sub>2</sub> (no catalyst) as well as in EF and PEF (0.50 mM Fe<sup>2+</sup> as catalyst), the solution pH underwent a slight fall from 3.0 to ~ 2.7-2.8 after 360 min of electrolysis, which can be ascribed to the production of acidic products such as carboxylic acids (Ruiz et al. 2011; Moreira et al. 2013; Florenza et al. 2014; Thiam et al. 2015a). A preliminary study with the same solution under a 6 W UVA irradiation in the absence of electric current confirmed that the substrate content did not vary with time, as expected if *trans*-cinnamic acid is not directly photolyzed by UVA light.

Fig. 1a depicts a very slow abatement of *trans*-cinnamic acid by AO-H<sub>2</sub>O<sub>2</sub>, requiring 360 min to completely disappear. The reaction rate of this compound with generated ROS, pre-eminently with BDD(•OH) originated from reaction (1), is then very low. In contrast, Fig. 1b depicts a much quicker decay and at similar rate in EF and PEF, being completely removed in about 42 min in both cases. The more rapid disappearance of this compound in such processes can be related to its faster reaction occurring in the bulk with •OH originated from Fenton's reaction (3) compared with the much slower attack of BDD(•OH) confined near the anode. The quite similar removal rate in EF and PEF can be explained by a very small contribution of the photolytic reaction (4) to produce greater quantities of •OH in the bulk.

The concentration decays of Figs. 1a and b were well fitted to a pseudo-first-order kinetic equation, as can be seen in the inset panels. This behavior suggests that *trans*-cinnamic acid is attacked by a steady concentration of BDD(•OH) and/or •OH in each treatment. From this analysis, apparent rate constants ( $k_1$ ) of 0.012 min<sup>-1</sup> (square regression coefficient  $R^2 = 0.991$ ) for AO-H<sub>2</sub>O<sub>2</sub>, 0.052 min<sup>-1</sup> ( $R^2 = 0.998$ ) for EF and 0.050 min<sup>-1</sup> ( $R^2 = 0.9990$ ) for PEF were obtained. The  $k_1$  value

1  
2 in EF and PEF was 4.2-4.3 orders of magnitude greater than that in AO-H<sub>2</sub>O<sub>2</sub>, corroborating the  
3 much larger oxidation ability of •OH compared to BDD(•OH) in the two former EAOPs.  
4

5 The study of the kinetic decay of *trans*-cinnamic acid was extended to lower concentrations of  
6 0.185 and 0.463 mM by applying 33.3 mA cm<sup>-2</sup>. Total removal of the substrate occurred at shorter  
7 time as the initial organic load decreased. For example, in AO-H<sub>2</sub>O<sub>2</sub>, *trans*-cinnamic acid  
8 disappeared at 270, 330 and 360 min for 0.185, 0.463 and 0.926 mM, respectively, whereas its  
9 removal in the EF treatment occurred at 8, 20 and 42 min for the same concentrations. According to  
10 this trend, a raising  $k_1$  value with decreasing substrate content was obtained from the corresponding  
11 pseudo-first-order kinetic analysis. Thus,  $k_1$  grew from 0.012 min<sup>-1</sup> ( $R^2 = 0.991$ ) to 0.014 min<sup>-1</sup> ( $R^2 =$   
12 0.992) in AO-H<sub>2</sub>O<sub>2</sub> and from 0.052 min<sup>-1</sup> ( $R^2 = 0.998$ ) to 0.58 min<sup>-1</sup> ( $R^2 = 0.994$ ) in EF when  
13 changing from 0.926 mM to 0.185 mM. It is then evident that the kinetic decay of this acid does not  
14 obey a true pseudo-first-order reaction, because similar  $k_1$  values should be found independently of  
15 its initial content. Since analogous quantities of BDD(•OH) and/or •OH are produced in each EAOP  
16 at  $j = 33.3$  mA cm<sup>-2</sup> as the organic load grows, a larger proportion of these oxidizing radicals is able  
17 to react with the oxidation products generated, thus decreasing their available quantity to attack the  
18 *trans*-cinnamic acid, eventually decelerating its removal.  
19  
20  
21  
22  
23  
24  
25  
26  
27  
28  
29  
30  
31  
32  
33  
34  
35  
36  
37  
38  
39

### 40 3.2. Mineralization of *trans*-cinnamic acid solutions by AO-H<sub>2</sub>O<sub>2</sub>, EF and PEF

41 For the above solutions with 0.926 mM *trans*-cinnamic acid of pH 3.0 treated by the EAOPs at  
42 33.3 mA cm<sup>-2</sup>, their TOC decay was determined in order to ascertain the relative mineralization  
43 ability. Fig. 2a highlights a slow and continuous TOC removal under AO-H<sub>2</sub>O<sub>2</sub> conditions, reaching  
44 a partial mineralization of 68% after 360 min of electrolysis. A much rapid TOC abatement can be  
45 observed in EF, with a final TOC reduction of 78%. It should be noted that the mineralization  
46 process in EF was very fast up to 120 min as a result of the efficient oxidation by •OH but, at longer  
47 time, it underwent a progressive deceleration suggesting the generation of more recalcitrant  
48 products, like Fe(III)-carboxylate complexes, which are very refractory to •OH and can only be  
49  
50  
51  
52  
53  
54  
55  
56  
57  
58  
59  
60  
61  
62  
63  
64  
65

1 slowly destroyed by BDD( $\bullet$ OH) (Sirés et al. 2014). Fig. 2a also evidences a very positive effect of  
2 UVA irradiation during the PEF process, which yielded a high TOC decay rate to attain an almost  
3 total mineralization with 98% TOC reduction at 360 min. This large acceleration of the  
4 mineralization process can be ascribed to the photolysis of products such as Fe(III)-carboxylate  
5 species via reaction (5) (Sirés et al. 2014; Brillas and Martínez-Huitle 2015). These findings  
6 indicate that the oxidation ability of the EAOPs to mineralize the *trans*-cinnamic acid increases in  
7 the sequence AO-H<sub>2</sub>O<sub>2</sub> < EF < PEF.  
8  
9

10 Fig. 2b shows the MCE values estimated from Eq. (7) for the assays of Fig. 2a. A higher  
11 current efficiency was obtained as the relative mineralization power of the EAOP increased. This  
12 tendency was more apparent between 60 and 120 min of electrolysis, because of the effect of  
13 BDD( $\bullet$ OH) and  $\bullet$ OH oxidation and photolysis on the mineralization rate in each treatment. In PEF,  
14 the MCE value dropped from 71% at the beginning of the treatment to 16% at 360 min. This fall in  
15 current efficiency can be explained by the production of more recalcitrant final oxidation products  
16 as well as the progressive loss of organic matter (Panizza and Cerisola 2009; Florenza et al. 2014;  
17 Thiam et al. 2015b). In the case of EF, the MCE value rose from an initial 14% to 28% at 120 min,  
18 further decaying to 13%. This is due to the initial formation of some persistent products that react  
19 slowly with  $\bullet$ OH in EF, requiring longer time for their mineralization, whereas their continuous  
20 removal caused the increase in MCE at the beginning of this process. In contrast, the MCE values in  
21 AO-H<sub>2</sub>O<sub>2</sub> remained practically constant between 13% and 15%, indicating a constant mineralization  
22 rate of products upon BDD( $\bullet$ OH) oxidation.  
23  
24  
25  
26  
27  
28  
29  
30  
31  
32  
33  
34  
35  
36  
37  
38  
39  
40  
41  
42  
43  
44  
45  
46  
47  
48  
49

#### 50 Effect of applied current density and substrate concentration on the performance of EAOPs

51 It is well known that the amount of oxidizing hydroxyl radicals acting in each EAOP is limited  
52 by the applied  $j$ . To clarify the influence of this key operation parameter, the mineralization of  
53 0.926 mM *trans*-cinnamic acid solutions was carried out at  $j$  in the range 16.7 - 100 mA cm<sup>-2</sup>. Figs.  
54  
55  
56  
57  
58  
59  
60  
61  
62  
63  
64  
65

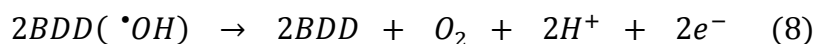
1  
2  
3  
4  
5  
6  
7  
8  
9  
10  
11  
12  
13  
14  
15  
16  
17  
18  
19  
20  
21  
22  
23  
24  
25  
26  
27  
28  
29  
30  
31  
32  
33  
34  
35  
36  
37  
38  
39  
40  
41  
42  
43  
44  
45  
46  
47  
48  
49  
50  
51  
52  
53  
54  
55  
56  
57  
58  
59  
60  
61  
62  
63  
64  
65

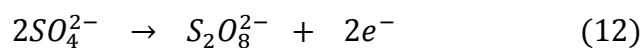
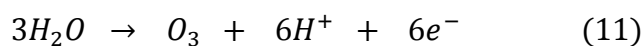
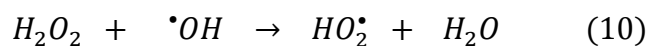
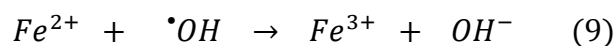
3a-c depict the TOC decay vs. electrolysis time measured in the AO-H<sub>2</sub>O<sub>2</sub>, EF and PEF assays, respectively. For the former process, Fig. 3a shows a quite similar TOC abatement at 16.7 - 66.7 mA cm<sup>-2</sup> during about 240 min, whereas the mineralization rate increased more significantly at 100 mA cm<sup>-2</sup>. This means that the expected rise in BDD(<sup>•</sup>OH) from the acceleration of reaction (1) at higher *j* (Sirés et al. 2014) has little influence on the destruction of organics, indicating that the excess of ROS produced are rather consumed in parasitic reactions, as will be discussed below. The influence of *j* in AO-H<sub>2</sub>O<sub>2</sub> was more apparent between 240 and 360 min, when final products like short-linear carboxylic acids are the main accumulated organics. At 360 min, for example, increasing TOC reductions of 64%, 68%, 76% and 84% for 16.7, 33.3, 66.7 and 100 mA cm<sup>-2</sup>, respectively, were found. A partial mineralization but with greater TOC decay can be seen in Fig. 3b for the comparative EF runs. In this process, higher *j* originated more quantities of BDD(<sup>•</sup>OH) as well as greater amounts of <sup>•</sup>OH in the bulk due to the quicker generation of H<sub>2</sub>O<sub>2</sub> by reaction (2) and the concomitant acceleration of Fenton's reaction (3). Both ROS then play a pre-eminent role to destroy the intermediates and their Fe(III) complexes and thus, greater TOC decay at higher *j* values can be clearly distinguished in Fig. 3b from 120 min of electrolysis. At the end of these treatments, however, the best *j* of 100 mA cm<sup>-2</sup> only yielded 90% mineralization. The behavior was very different when PEF was applied. Fig. 3c reveals that the low production of BDD(<sup>•</sup>OH) and <sup>•</sup>OH at 16.7 mA cm<sup>-2</sup> impeded the complete production of photosensitive products and, therefore, only 91% TOC reduction was achieved at 360 min. In contrast, the use of *j* ≥ 33.3 mA cm<sup>-2</sup> favored an effective generation of oxidants, and nearly all the accumulated products were photosensitive and were removed at similar rate yielding an almost total mineralization with 97-98% TOC reduction at the end of all the treatments. These findings indicate that 33.3 mA cm<sup>-2</sup> can be considered as the best *j* value for the application of this EAOP to degrade a 0.926 mM *trans*-cinnamic solution.

Figs. 4a-c show a loss in current efficiency for each EAOP as *j* rose. This tendency is not surprising in view of the low effect of this parameter on the TOC decay of all the treatments, mainly

1 in AO-H<sub>2</sub>O<sub>2</sub> and PEF (see Figs. 3a and c). As shown in Fig. 4a, the MCE values in each AO-H<sub>2</sub>O<sub>2</sub>  
2 at a given  $j \geq 33.3 \text{ mA cm}^{-2}$  basically remained unchanged during each run, as expected for a  
3 constant mineralization rate of intermediates, whereas at  $16.7 \text{ mA cm}^{-2}$ , it gradually dropped from  
4 39% to 21% due to the smaller mineralization ability of the lower amounts of BDD( $\bullet$ OH) generated.  
5 For EF, a maximum MCE value was attained after 90-120 min of all the assays (see Fig. 4b),  
6 corroborating the initial formation of several products that are slowly destroyed by hydroxyl  
7 radicals while their gradual mineralization largely improves the current efficiency at the beginning  
8 of the process. The same phenomenon is shown in Fig. 4c for PEF at  $16.7 \text{ mA cm}^{-2}$ , since the  
9 smaller amounts of BDD( $\bullet$ OH) and  $\bullet$ OH produced under these conditions attack slowly the  
10 substrate and its products and low quantities of photosensitive species are formed to be removed by  
11 UVA light. Current efficiency then grew as these initial recalcitrant products progressively  
12 disappeared from the medium. This behavior was not found for greater  $j$  values because the  
13 mineralization was enhanced by the faster photolysis of larger quantities of products, like Fe(III)-  
14 carboxylate species. In all the EF and PEF assays, the current efficiency diminished at long  
15 electrolysis time due to two main contributions, the loss of organic load and the formation of more  
16 recalcitrant intermediates, as stated above. For the most powerful EAOP, i.e., PEF process,  
17 maximum MCE of  $\sim 71$ -73% was obtained after 90 and 30 min at  $16.7$  and  $33.3 \text{ mA cm}^{-2}$ .  
18  
19  
20  
21  
22  
23  
24  
25  
26  
27  
28  
29  
30  
31  
32  
33  
34  
35  
36  
37  
38  
39  
40  
41

42 The decay in MCE as  $j$  grows is typical of EAOPs and can be associated with the consumption  
43 of the excess of generated hydroxyl radicals by waste reactions. For example, the anodic oxidation  
44 of physisorbed BDD( $\bullet$ OH) to O<sub>2</sub> via reaction (8) and the removal of  $\bullet$ OH by Fe<sup>2+</sup> and H<sub>2</sub>O<sub>2</sub> via  
45 reactions (9) and (10), respectively (Sirés and Brillas 2012; Sirés et al. 2014). It is also expected that  
46 the formation of other weaker oxidants at the BDD anode such as ozone via reaction (11) and  
47 S<sub>2</sub>O<sub>8</sub><sup>2-</sup> ion from SO<sub>4</sub><sup>2-</sup> ion of the electrolyte via reaction (12), thereby inhibiting the H<sub>2</sub>O discharge  
48 from reaction (1) (Panizza and Cerisola 2009), become largely enhanced as well.  
49  
50  
51  
52  
53  
54  
55  
56  
57  
58  
59





Another important operation parameter in the EAOPs is the substrate concentration since it determines the oxidation ability of hydroxyl radicals and/or their combined action with the photo-oxidation by UVA light. The influence of this parameter was examined for 0.185, 0.463, 0.926 and 1.852 mM of *trans*-cinnamic acid at the best  $j = 33.3 \text{ mA cm}^{-2}$  found for PEF, and the results are presented in Figs. 5a-c. Oscillating final percentages of TOC removal were always found for each EAOP with increasing substrate content. For example, at the end of the above treatments, TOC was reduced by 68-81% in AO-H<sub>2</sub>O<sub>2</sub>, 75-81% in EF and 87-97% in PEF. Note that quite analogous percentages of TOC abatement were found for the two former treatments up to 0.463 mM, thus showing similar final mineralization values.

For the above assays, however, greater amounts of TOC were always removed with raising the organic load of the solution and this fact is reflected in Figs. 6a-c from the concomitant enhancement of the corresponding MCE values. At 120 min, for example, operating between 0.185 and 1.852 mM *trans*-cinnamic acid, the current efficiency gradually grew from 3.6% to 38%, from 5.1% to 53% and from 8.6% to 60% in AO-H<sub>2</sub>O<sub>2</sub>, EF and PEF, respectively. These findings confirm again that the relative oxidation ability of these EAOPs always increased in the sequence AO-H<sub>2</sub>O<sub>2</sub> < EF < PEF. As mentioned above, similar quantities of BDD( $\cdot$ OH) and/or  $\cdot$ OH are expected to be generated in each EAOP at  $33.3 \text{ mA cm}^{-2}$ . Consequently, one can infer that a larger organic load favors the reaction of higher quantities of these oxidizing species with intermediates, with deceleration of the waste reactions (8)-(12). The quicker formation of products also enhanced the PEF process because the resulting photosensitive species can be more rapidly removed upon

1 UVA irradiation. Nevertheless, the most concentrated solution was only mineralized up to a 92% by  
2 this procedure, a value lower than 98% obtained for 0.463 and 0.962 mM solutions, where lower  
3 amounts of undesired persistent products are finally accumulated. Figs. 6b and c highlight again the  
4 fall of current efficiency at prolonged electrolysis because of both, the gradual generation of highly  
5 recalcitrant products and the loss of organic matter, as pointed out above.  
6  
7  
8  
9  
10

11 All these findings allow concluding that the most convenient conditions for applying the PEF  
12 process involve the treatment of 0.926 mM *trans*-cinnamic at 33.3 mA cm<sup>-2</sup>, since this yielded the  
13 greatest mineralization with 98% TOC removal and an acceptable current efficiency of 16% during  
14 final stages. Higher current values did not accelerate the process and produced a significant MCE  
15 decay. The use of more concentrated solutions is not beneficial because of the lower TOC removal.  
16  
17  
18  
19  
20  
21  
22  
23  
24

#### 25 Identification of products and evolution of generated carboxylic acids

26

27 Table 1 summarizes the characteristics of five primary aromatics and one heteroaromatic  
28 product of *trans*-cinnamic acid (**1**) identified by GC-MS after 30 and 90 min of AO-H<sub>2</sub>O<sub>2</sub> treatment  
29 of a 0.926 mM substrate solution at pH 3.0 and 33.3 mA cm<sup>-2</sup>. While the heteroaromatic **2** arises  
30 from an internal cyclization of the carboxylic group of **1**, the aldehyde **3** is produced from its  
31 decarboxylation and the acid **4** from the oxidation of its double bond to a single one. Further  
32 degradation of **3** yields compounds **5-7**.  
33  
34  
35  
36  
37  
38  
39  
40  
41  
42

43 It is expected that the cleavage of the benzene ring of the above compounds leads to linear  
44 products that evolve to short-linear aliphatic carboxylic acids (El-Ghenymy et al. 2014; Sirés et al.  
45 2014). This possibility was corroborated by ion-exclusion HPLC analysis of the solutions degraded  
46 under the conditions of Fig. 2. Fumaric (**8**), acetic (**9**) and oxalic (**10**) acids were detected in these  
47 chromatograms allowing the quantification of their concentrations during the electrolysis. Acid **10**  
48 was also identified by GC-MS as a deprotonated ion with m/z 89 (see Table 1). Note that the final  
49 acids **8** and **9** are oxidized to the ultimate acid **10**, which is directly converted into CO<sub>2</sub> (Ruiz et al.  
50 2011; Sirés and Brillas 2012). These acids form Fe(III) complexes to a large extent in EF and PEF,  
51  
52  
53  
54  
55  
56  
57  
58  
59  
60  
61  
62  
63  
64  
65

1 being slowly oxidized by BDD( $\bullet$ OH) and more hardly attacked by  $\bullet$ OH (Moreira et al. 2013;  
2 Florenza et al. 2014; Thiam et al. 2015a).  
3

4  
5 Traces of acid **8** ( $< 0.0043$  mM) appeared until 120 min of all treatments, whereas small  
6 contents of acid **9** were only found after 180 min of AO-H<sub>2</sub>O<sub>2</sub>. These compounds and their Fe(III)  
7 complexes were then rapidly removed by hydroxyl radicals. In contrast, Fig. 7 shows that the final  
8 acid **10** was much more largely accumulated in all the EAOPs, then being the main carboxylic acid  
9 generated during the mineralization process of *trans*-cinnamic acid. In AO-H<sub>2</sub>O<sub>2</sub>, this acid was  
10 progressively accumulated up to 0.137 mM as maximal at 180 min, whereupon it decayed to 0.094  
11 mM. This value accounts for 2.3 mg L<sup>-1</sup> TOC, only contributing in 7.2% to the organic load of the  
12 remaining solution (32 mg L<sup>-1</sup> TOC, see Fig. 2). This means that the majority of components (93%)  
13 of such solution were recalcitrant products that are slowly destroyed by BDD( $\bullet$ OH). On the other  
14 hand, Fig. 7 reveals a very high accumulation of acid **10** up to 0.86 mM at 60 min in EF and 1.02  
15 mM at 40 min in PEF as a result of the much faster destruction of primary intermediates by  $\bullet$ OH. At  
16 longer time, the evolution of this acid depended on the characteristics of each treatment. In EF, the  
17 slow oxidation of Fe(III)-oxalate species mainly by BDD( $\bullet$ OH) yielded 0.38 mM of **10**, related to  
18 9.1 mg L<sup>-1</sup> TOC and a 41% of the 22 mg L<sup>-1</sup> TOC of the final solution (see Fig. 2). The remaining  
19 solution of EF then contained 59% of undetected products that are highly recalcitrant to hydroxyl  
20 radicals. Conversely, the UVA irradiation used in PEF led to rapid and total photodecarboxylation  
21 of Fe(III)-oxalate complexes via reaction (5), with all the acid **10** disappearing in only 240 min,  
22 although the final solution at 360 min still contained a 2% of the starting TOC (see Fig. 2). One can  
23 infer that the PEF process destroys most of persistent products that cannot be oxidized by hydroxyl  
24 radicals in EF, thanks to the photolytic action of UVA light. This behavior along with the total  
25 removal of final carboxylic acids justifies the almost total mineralization achieved in PEF.  
26  
27  
28  
29  
30  
31  
32  
33  
34  
35  
36  
37  
38  
39  
40  
41  
42  
43  
44  
45  
46  
47  
48  
49  
50  
51  
52  
53  
54  
55  
56  
57  
58  
59  
60  
61  
62  
63  
64  
65



## Degradation route for *trans*-cinnamic acid by EAOPs with BDD

Based on the products identified in this work, a plausible route for *trans*-cinnamic acid mineralization by EAOPs with a BDD anode is proposed in Fig. 8. The oxidation of the substrate and its aromatic and heteroaromatic products occurs by reaction with BDD( $\bullet$ OH) in AO-H<sub>2</sub>O<sub>2</sub> and more rapidly with  $\bullet$ OH in EF and PEF. The final carboxylic acids and Fe(III)-carboxylate species are preferentially attacked by BDD( $\bullet$ OH). Other generated oxidants like H<sub>2</sub>O<sub>2</sub>, HO<sub>2</sub> $\bullet$ , O<sub>3</sub> and S<sub>2</sub>O<sub>8</sub><sup>2-</sup> can oxidize much more slowly some of the products as well. In the proposed path, only the fate of Fe(III)-oxalate complexes is specified for the sake of simplicity.

The route is initiated by the attack of hydroxyl radicals over **1** to cause: (i) an internal cyclization of its carboxylic group producing the heteroaromatic **2**, (ii) its decarboxylation followed by oxidation to generate the aldehyde **3** and (iii) the transformation of its double bond giving the saturated carboxylic acid **4**. Subsequent oxidation of **3** yields the saturated acid **5** and benzaldehyde **6**, which is then oxidized to benzoic acid **7**. Further cleavage of the benzene ring of all the above compounds gives a mixture of final acids **8-10**. Acids **8** and **9**, formed to a small extent, are rapidly converted into acid **10**. This acid is transformed into CO<sub>2</sub> by BDD( $\bullet$ OH) in AO-H<sub>2</sub>O<sub>2</sub>, whereas in EF and PEF, it forms Fe(III)-oxalate species that are slowly mineralized by BDD( $\bullet$ OH) and much more quickly photodecarboxylated by UVA light with Fe<sup>2+</sup> regeneration via reaction (5).

## Conclusions

The PEF degradation of 0.926 mM *trans*-cinnamic acid solutions of pH 3.0 led to an almost total mineralization at  $j \geq 33.3$  mA cm<sup>-2</sup>. PEF is much more powerful than EF, which yielded 90% TOC abatement as maximal at 100 mA cm<sup>-2</sup>, because of the quick photodegradation of highly recalcitrant products like Fe(III)-carboxylate complexes. The oxidation power of AO-H<sub>2</sub>O<sub>2</sub> was always lower than that of EF, indicating the positive combination of BDD( $\bullet$ OH) produced at the anode and  $\bullet$ OH formed from Fenton's reaction to remove organics. For each EAOP, increasing  $j$

1  
2  
3  
4  
5  
6  
7  
8  
9  
10  
11  
12  
13  
14  
15  
16  
17  
18  
19  
20  
21  
22  
23  
24  
25  
26  
27  
28  
29  
30  
31  
32  
33  
34  
35  
36  
37  
38  
39  
40  
41  
42  
43  
44  
45  
46  
47  
48  
49  
50  
51  
52  
53  
54  
55  
56  
57  
58  
59  
60  
61  
62  
63  
64  
65

from 16.7 to 100 mA cm<sup>-2</sup> caused more rapid mineralization with lower current efficiency, whereas the use of more concentrated solutions from 0.185 to 1.852 mM enhanced the amount of TOC abated, which caused a gradual rise of current efficiency at long electrolysis time. Five primary aromatics, one heteroaromatic and three short final carboxylic acids were identified. Oxalic acid was the most important final product. It presented a large persistence in AO-H<sub>2</sub>O<sub>2</sub> and EF, but disappeared rapidly in PEF due to the quick photolysis of its Fe(III) complexes that explains the superior oxidation power of this EAOP.

**Acknowledgments** Financial support from MINECO (Ministerio de Economía y Competitividad, Spain) under project CTQ2013-48897-C2-1-R, co-financed with FEDER funds, and the Ph.D. fellowship awarded to N. Flores by SENESCYT (Secretaría Nacional de Educación Superior, Ciencia, Tecnología e Innovación, Ecuador) are acknowledged.

## References

- Assumpção MHMT, Moraes A, De Souza RFB, Reis RM, Rocha RS, Gaubeur I, Calegaro ML, Hammer P, Lanza MRV, Santos MC (2013) Degradation of dipyrone via advanced oxidation processes using a cerium nanostructured electrocatalyst material, *Appl Catal A-Gen* 462-463:256-261.
- Borràs N, Oliver R, Arias C, Brillas E (2010) Degradation of atrazine by electrochemical advanced oxidation processes using a boron-doped diamond anode. *J Phys Chem A* 114(24):6613-6621.
- Boye B, Dieng MM, Brillas E (2003) Electrochemical degradation of 2,4,5-trichlorophenoxyacetic acid in aqueous medium by peroxi-coagulation. Effect of pH and UV light. *Electrochim Acta* 48(7):781-790.

- 1  
2 Brillas E, Martínez-Huitle CA (2015) Decontamination of wastewaters containing synthetic organic  
3 dyes by electrochemical methods. An updated review. *Appl Catal B-Environ* 166-167:603-  
4 643.  
5  
6  
7 Cavalcanti EB, Garcia-Segura S, Centellas F, Brillas E (2013) Electrochemical incineration of  
8 omeprazole in neutral aqueous medium using a platinum or boron-doped diamond.  
9 Degradation kinetics and oxidation products. *Water Res* 47(5):1803-1815.  
10  
11  
12 Chatzisymeon E, Dimou A, Mantzavinos D, Katsaounis A (2009) Electrochemical oxidation of  
13 model compounds and olive mill wastewater over DSA electrodes: 1. The case of Ti/IrO<sub>2</sub>  
14 anode. *J Hazard Mater* 167(1-3):268-274.  
15  
16  
17 Ciríaco L, Anjo C, Correia J, Pacheco MJ, Lopes A (2009) Electrochemical degradation of  
18 ibuprofen on Ti/Pt/PbO<sub>2</sub> and Si/BDD electrodes. *Electrochim Acta* 54(5):1464-1472.  
19  
20  
21 Cruz-González K, Torres-López O, García-León A, Brillas E, Hernández-Ramírez A, Peralta-  
22 Hernández JM (2012) Optimization of electro-Fenton/BDD process for decolorization of a  
23 model azo dye wastewater by means of response surface methodology. *Desalination* 286:63-  
24 68.  
25  
26  
27 Cruz-González K, Torres-López O, García-León A, Guzmán-Mar JL, Reyes LH, Hernández-  
28 Ramírez A, Peralta-Hernández JM (2010) Determination of optimum operating parameters for  
29 Acid Yellow 36 decolorization by electro-Fenton process using BDD cathode. *Chem Eng J*  
30 160(1):199-206.  
31  
32  
33  
34  
35  
36 Deeb AA, Fayyad MK, Alawi MA (2012) Separation of polyphenols from Jordanian olive oil mill  
37 wastewater. *Cromatogr Res Int* Article ID 812127, 8 pp.  
38  
39  
40  
41  
42  
43  
44  
45  
46  
47  
48  
49  
50  
51 Di Gioia D, Bertin L, Fava F, Marchetti L (2001) Biodegradation of hydroxylated and methoxylated  
52 benzoic, phenylacetic and phenylpropenoic acids present in olive mill wastewaters by two  
53 bacterial strains. *Res Microbiol* 152(1):83-93.  
54  
55  
56  
57  
58  
59  
60  
61  
62  
63  
64  
65

- 1  
2  
3  
4  
5  
6  
7  
8  
9  
10  
11  
12  
13  
14  
15  
16  
17  
18  
19  
20  
21  
22  
23  
24  
25  
26  
27  
28  
29  
30  
31  
32  
33  
34  
35  
36  
37  
38  
39  
40  
41  
42  
43  
44  
45  
46  
47  
48  
49  
50  
51  
52  
53  
54  
55  
56  
57  
58  
59  
60  
61  
62  
63  
64  
65
- Dirany A, Sirés I, Oturan N, Özcan A, Oturan MA (2012) Electrochemical treatment of the antibiotic sulfachloropyridazine: kinetics, reaction pathways, and toxicity evolution. *Environ Sci Technol* 46(7):4074-4082.
- El-Ghenymy A, Rodríguez RM, Brillas E, Oturan N, Oturan MA (2014) Electro-Fenton degradation of the antibiotic sulfanilamide with Pt/carbon-felt and BDD/carbon-felt cells. Kinetics, reaction intermediates, and toxicity assessment. *Environ Sci Pollut Res* 21(14):8368-8378.
- Florenza X, Solano AMS, Centellas F, Martínez-Huitle CA, Brillas E, Garcia-Segura S (2014) Degradation of the azo dye Acid Red 1 by anodic oxidation and indirect electrochemical processes based on Fenton's reaction chemistry. Relationship between decolorization, mineralization and products. *Electrochim Acta* 142:276-288.
- Guinea E, Brillas E, Centellas F, Cañizares P, Rodrigo MA, Saez C (2009) Oxidation of enrofloxacin with conductive-diamond electrochemical oxidation, ozonation and Fenton oxidation. A comparison. *Water Res* 43(8):2131-2138.
- Hakkim FL, Miura M, Matsuda N, Alharassi AS, Guillemin G, Yamauchi M, Arivazhagan G, Song H (2014) An in vitro evidence for caffeic acid, rosmarinic acid and *trans*-cinnamic acid as a skin protectant against  $\gamma$ -radiation. *Int J Low Rad* 9(4):305-316.
- Hojati M, Modarres-Sanavy SAM, Enferadi ST, Majdi M, Ghanati F, Farzadfar S (2015) Differential deployment of parthenolide and phenylpropanoids in feverfew plants subjected to divalent heavy metals and *trans*-cinnamic acid. *Plant Soil* DOI:10.1007/s11104-015-2677-0.
- Khataee A, Akbarpour A, Vahi B (2014) Photoassisted electrochemical degradation of an azo dye using Ti/RuO<sub>2</sub> anode and carbon nanotubes containing gas-diffusion cathode. *J Taiwan Inst Chem Eng* 45(3):930-936.
- Khataee A, Khataee A, Fathinia M, Vahid B, Joo SW (2013) Kinetic modeling of photoassisted-electrochemical process for degradation of an azo dye using boron-doped diamond anode and cathode with carbon nanotubes. *J Ind Eng Chem* 19(6):1890-1894.

- 1  
2  
3  
4  
5  
6  
7  
8  
9  
10  
11  
12  
13  
14  
15  
16  
17  
18  
19  
20  
21  
22  
23  
24  
25  
26  
27  
28  
29  
30  
31  
32  
33  
34  
35  
36  
37  
38  
39  
40  
41  
42  
43  
44  
45  
46  
47  
48  
49  
50  
51  
52  
53  
54  
55  
56  
57  
58  
59  
60  
61  
62  
63  
64  
65
- Kontos SS, Koutsoukos PG, Paraskeva CA (2014) Removal and recovery of phenolic compounds from olive mill wastewater by cooling crystallization. *Chem Eng J* 251:319-328.
- Lafont F, Garcia IM, Aramendia MA, Marinas JM, Urbano FJ, Fernandez JM, Marti V (2001) Automated on-line solid-phase extraction and HPLC-mass spectrometry for rapid determination of phenolic compounds found in olive mill wastewaters. *Adv Mass Spectrom* 15:875-876.
- Letizia CS, Cocchiara J, Lapczynski A, Lalko J, Api AM (2005) Fragrance material review on cinnamic acid. *Food Chem Toxicol* 43(6):925-943.
- Lopes RJG, Quinta-Ferreira RM (2010) Assessment of CFD-VOF method for trickle-bed reactor modeling in the catalytic wet oxidation of phenolic wastewater. *Ind Eng Chem Res* 49(6):2638-2648.
- Lopes RJG, Silva AMT, Quinta-Ferreira RM (2007) Screening of catalysts and effect of temperature for kinetic degradation studies of aromatic compounds during wet oxidation. *Appl Catal B-Environ* 73(1-2):193-202.
- Marselli B, Garcia-Gomez J, Michaud PA, Rodrigo MA, Comninellis C (2003) Electrogeneration of hydroxyl radicals on boron-doped diamond electrodes. *J Electrochem Soc* 150(3):D79-D83.
- Martínez-Huitle CA, Ferro S (2006) Electrochemical oxidation of organic pollutants for the wastewater treatment: direct and indirect processes. *Chem Soc Rev* 35(12):1324-1340.
- Moreira FC, Garcia-Segura S, Vilar VJP, Boaventura RAR, E. Brillas E (2013) Decolorization and mineralization of Sunset Yellow FCF azo dye by anodic oxidation, electro-Fenton, UVA photoelectro-Fenton and solar photoelectro-Fenton processes. *Appl Catal B-Environ* 142-143:877-890.
- Panizza M, Cerisola G (2009) Direct and mediated anodic oxidation of organic pollutants. *Chem Rev* 109(12):6541-6569.

- 1  
2  
3  
4  
5  
6  
7  
8  
9  
10  
11  
12  
13  
14  
15  
16  
17  
18  
19  
20  
21  
22  
23  
24  
25  
26  
27  
28  
29  
30  
31  
32  
33  
34  
35  
36  
37  
38  
39  
40  
41  
42  
43  
44  
45  
46  
47  
48  
49  
50  
51  
52  
53  
54  
55  
56  
57  
58  
59  
60  
61  
62  
63  
64  
65
- Rodrigo MA, Cañizares P, Sánchez-Carretero A, Sáez C (2010) Use of conductive-diamond electrochemical oxidation for wastewater treatment. *Catal Today* 151(1-2):173-177.
- Ruiz EJ, Hernández-Ramírez A, Peralta-Hernández JM, Arias C, Brillas E (2011) Application of solar photoelectro-Fenton technology to azo dyes mineralization: Effect of current density,  $\text{Fe}^{2+}$  and dye concentrations. *Chem Eng J* 171(2):385-392.
- Sanchez I, Stüber F, Fabregat A, Font J, Fortuny A, Bengoa C (2012) Degradation of model olive mill contaminants of OMW catalysed by zero-valent iron enhanced with a chelant. *J Hazard Mater* 199-200:328-335.
- Sirés I, Brillas E (2012) Remediation of water pollution caused by pharmaceutical residues based on electrochemical separation and degradation technologies: a review. *Environ Int* 40:212-229.
- Sirés I, Brillas E, Oturan MA, Rodrigo MA, Panizza M (2014) Electrochemical advanced oxidation processes: today and tomorrow. A review. *Environ Sci Pollut Res* 21(14):8336-8367.
- Thiam A, Sirés I, Centellas F, Cabot PL, Brillas E (2015a) Decolorization and mineralization of Allura Red AC azo dye by solar photoelectro-Fenton: Identification of intermediates. *Chemosphere* 136:1-8.
- Thiam A, Sirés I, Garrido JA, Rodríguez RM, Brillas E (2015b) Decolorization and mineralization of Allura Red AC aqueous solutions by electrochemical advanced oxidation processes, *J Hazard Mater* 290:34-42.
- Thiam A, Zhou M, Brillas E, Sirés I (2014) Two-step mineralization of Tartrazine solutions: Study of parameters and by-products during the coupling of electrocoagulation with electrochemical advanced oxidation processes. *Appl Catal B-Environ* 150-151:116-125.
- Vasudevan S, Oturan MA (2014) Electrochemistry: As cause and cure in water pollution-an overview. *Environ Chem Lett* 12(1):97-108.

1  
2  
3  
4  
5  
6  
7  
8  
9  
10  
11  
12  
13  
14  
15  
16  
17  
18  
19  
20  
21  
22  
23  
24  
25  
26  
27  
28  
29  
30  
31  
32  
33  
34  
35  
36  
37  
38  
39  
40  
41  
42  
43  
44  
45  
46  
47  
48  
49  
50  
51  
52  
53  
54  
55  
56  
57  
58  
59  
60  
61  
62  
63  
64  
65

Vatanpour V, Daneshvar N, Rasoulifard MH (2009) Electro-Fenton degradation of synthetic dye mixture: influence of intermediates. *J Environ Eng Manage* 19(1):277-282.

Wang A, Qu J, Liu H, Ru R (2008) Mineralization of an azo dye Acid Red 14 by photoelectro-Fenton process using an activated carbon fiber cathode. *Appl Catal B-Environ* 84(3-4):393-399.

Yahya MS, Oturan N, El Kacemi K, El Karbane M, Aravindakumar CT, Oturan MA (2014) Oxidative degradation study on antimicrobial agent ciprofloxacin by electro-Fenton process: Kinetics and oxidation products. *Chemosphere* 117:447-454.

Zeni ALB, de Albuquerque CAC, Goncalves F, Latini A, Tasca CI, Podesta R, Pagliosa CM, Duarte FS, de Lima TCM, Maraschin M (2013) Phytochemical profile, toxicity and antioxidant activity of *Aloysia gratissima* (Verbenaceae). *Quim Nova* 36(1):69-73.

## Figure captions

**Fig. 1** *trans*-Cinnamic acid content vs. electrolysis time for the degradation of 100 mL of a 0.926 mM substrate solution in 0.05 M Na<sub>2</sub>SO<sub>4</sub> at pH 3.0 and 25 °C using a BDD/air-diffusion cell of 3 cm<sup>2</sup> electrode area at 33.3 mA cm<sup>-2</sup>. In (a), anodic oxidation with electrogenerated H<sub>2</sub>O<sub>2</sub> (AO-H<sub>2</sub>O<sub>2</sub>). In (b), (■) electro-Fenton (EF) with 0.50 mM Fe<sup>2+</sup> and (▲) photoelectro-Fenton (PEF) with 0.50 mM Fe<sup>2+</sup> using a 6 W UVA light. The pseudo-first-order kinetic analysis for the *trans*-cinnamic acid concentration abatement is shown in the inset panels

**Fig. 2** (a) TOC removal and (b) variation of mineralization current efficiency with electrolysis time under the conditions of Fig. 1. Method: (●) AO-H<sub>2</sub>O<sub>2</sub>, (■) EF and (▲) PEF

**Fig. 3** Effect of current density on TOC decay vs. electrolysis time for the treatment of 100 mL of a 0.926 mM *trans*-cinnamic acid solution in 0.05 M Na<sub>2</sub>SO<sub>4</sub> at pH 3.0 and 25 °C using a BDD/air-diffusion cell. Method: (a) AO-H<sub>2</sub>O<sub>2</sub>, (b) EF and (c) PEF. Applied current density: (●) 16.7 mA cm<sup>-2</sup>, (▲) 33.3 mA cm<sup>-2</sup>, (◆) 66.7 mA cm<sup>-2</sup> and (▼) 100 mA cm<sup>-2</sup>

**Fig. 4** Mineralization current efficiency vs. electrolysis time for the trials of Fig. 3

**Fig. 5** Effect of *trans*-cinnamic acid concentration on TOC removal with electrolysis time for the degradation of 100 mL of solutions of this substrate in 0.05 M Na<sub>2</sub>SO<sub>4</sub> at pH 3.0 using a BDD/air-diffusion cell at 33.3 mA cm<sup>-2</sup> and 25 °C. Method: (a) AO-H<sub>2</sub>O<sub>2</sub>, (b) EF and (c) PEF. Content of *trans*-cinnamic acid: (●) 0.185 mM, (◆) 0.463 mM, (▲) 0.926 mM and (■) 1.852 mM

**Fig. 6** Variation of mineralization current efficiency with electrolysis time for the experiments given in Fig. 5

**Fig. 7** Time-course of the concentration of oxalic acid (10) detected during the treatments shown in Fig. 2. Method: (●) AO-H<sub>2</sub>O<sub>2</sub>, (■) EF and (▲) PEF



**Fig. 8** Route for *trans*-cinnamic acid mineralization by AO-H<sub>2</sub>O<sub>2</sub>, EF and PEF using a BDD/air-diffusion cell. The species •OH in the sequence of aromatics represents their oxidation by BDD(•OH) at the BDD surface and/or •OH from Fenton's reaction in the bulk

1  
2  
3  
4  
5  
6  
7  
8  
9  
10  
11  
12  
13  
14  
15  
16  
17  
18  
19  
20  
21  
22  
23  
24  
25  
26  
27  
28  
29  
30  
31  
32  
33  
34  
35  
36  
37  
38  
39  
40  
41  
42  
43  
44  
45  
46  
47  
48  
49  
50  
51  
52  
53  
54  
55  
56  
57  
58  
59  
60  
61  
62  
63  
64  
65

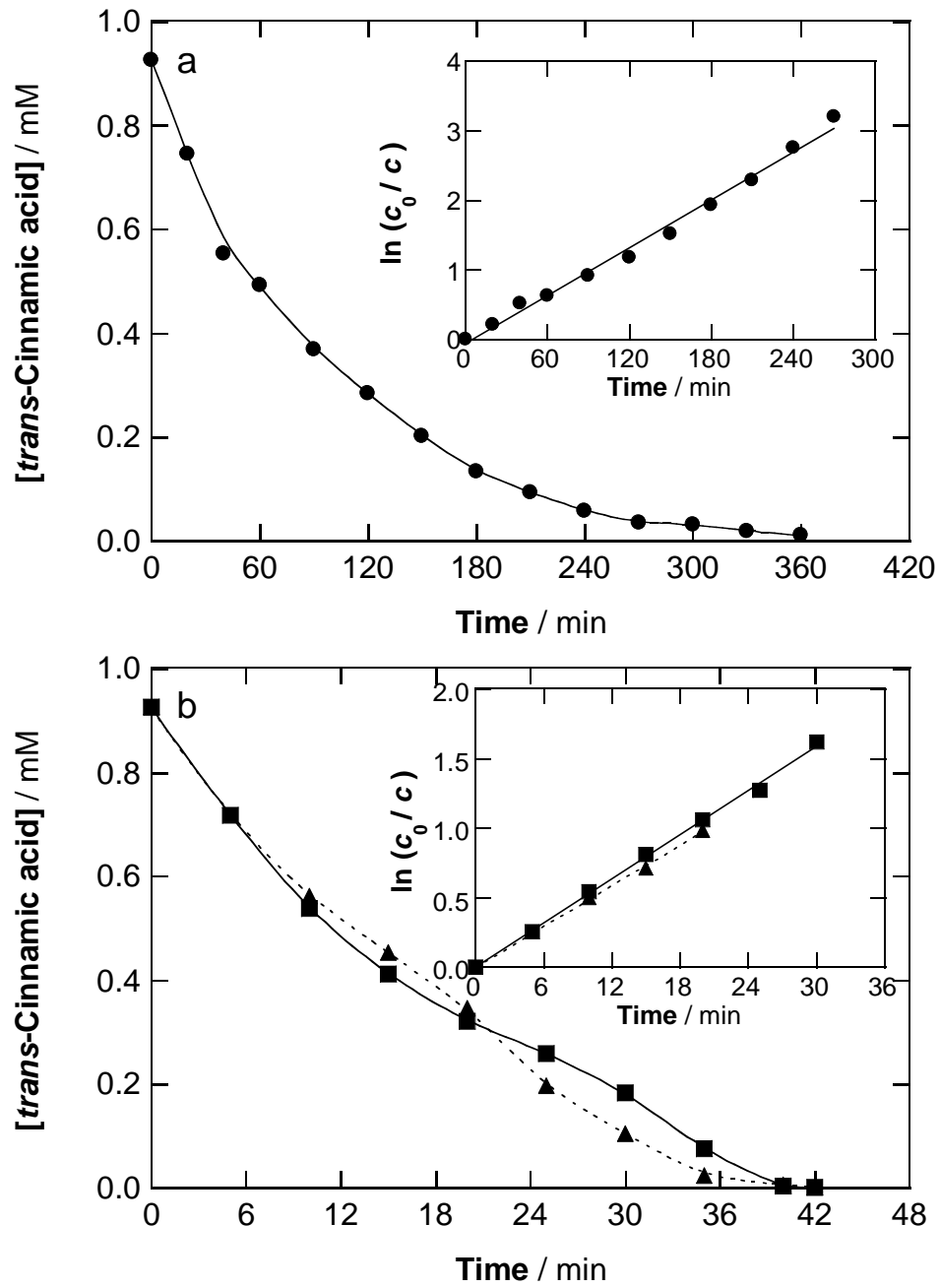


Fig. 1

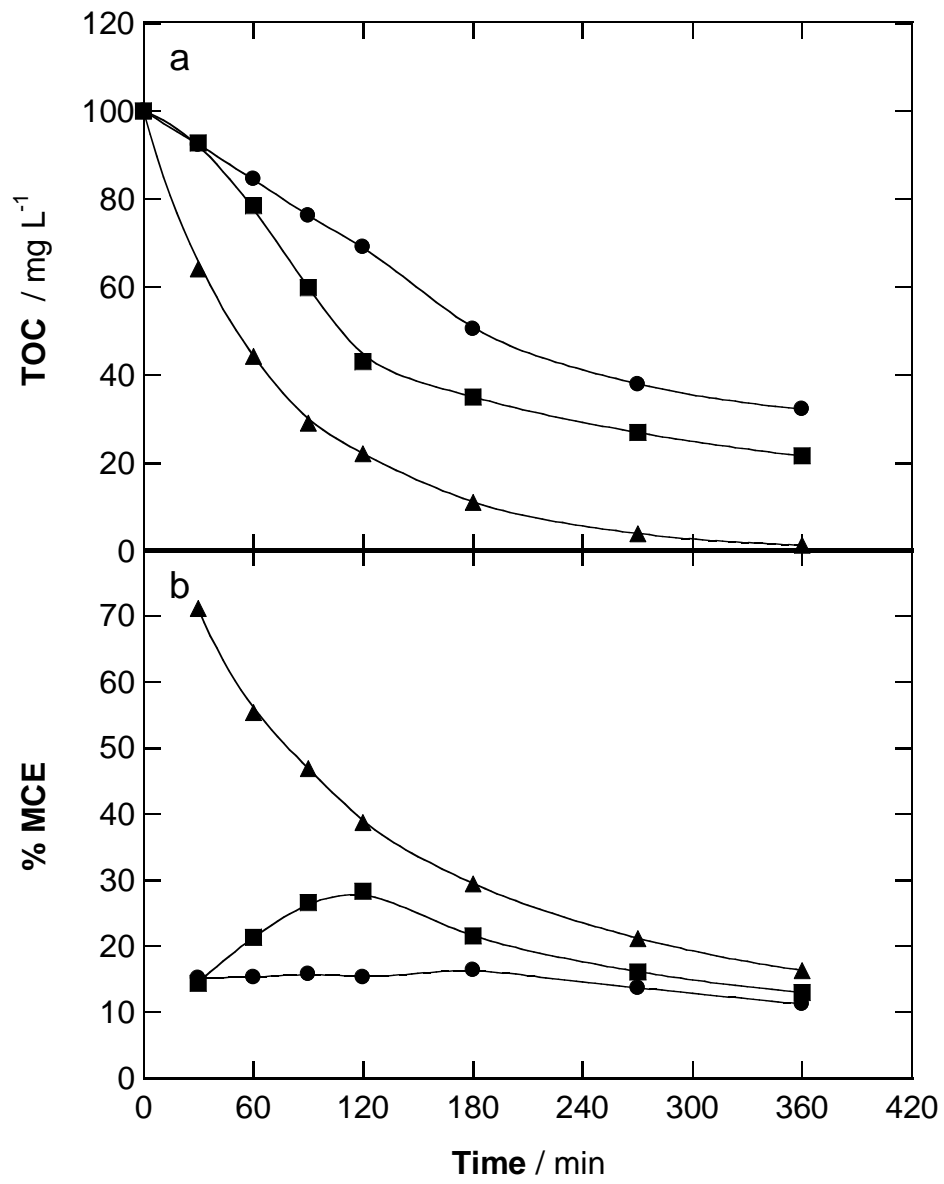


Fig. 2

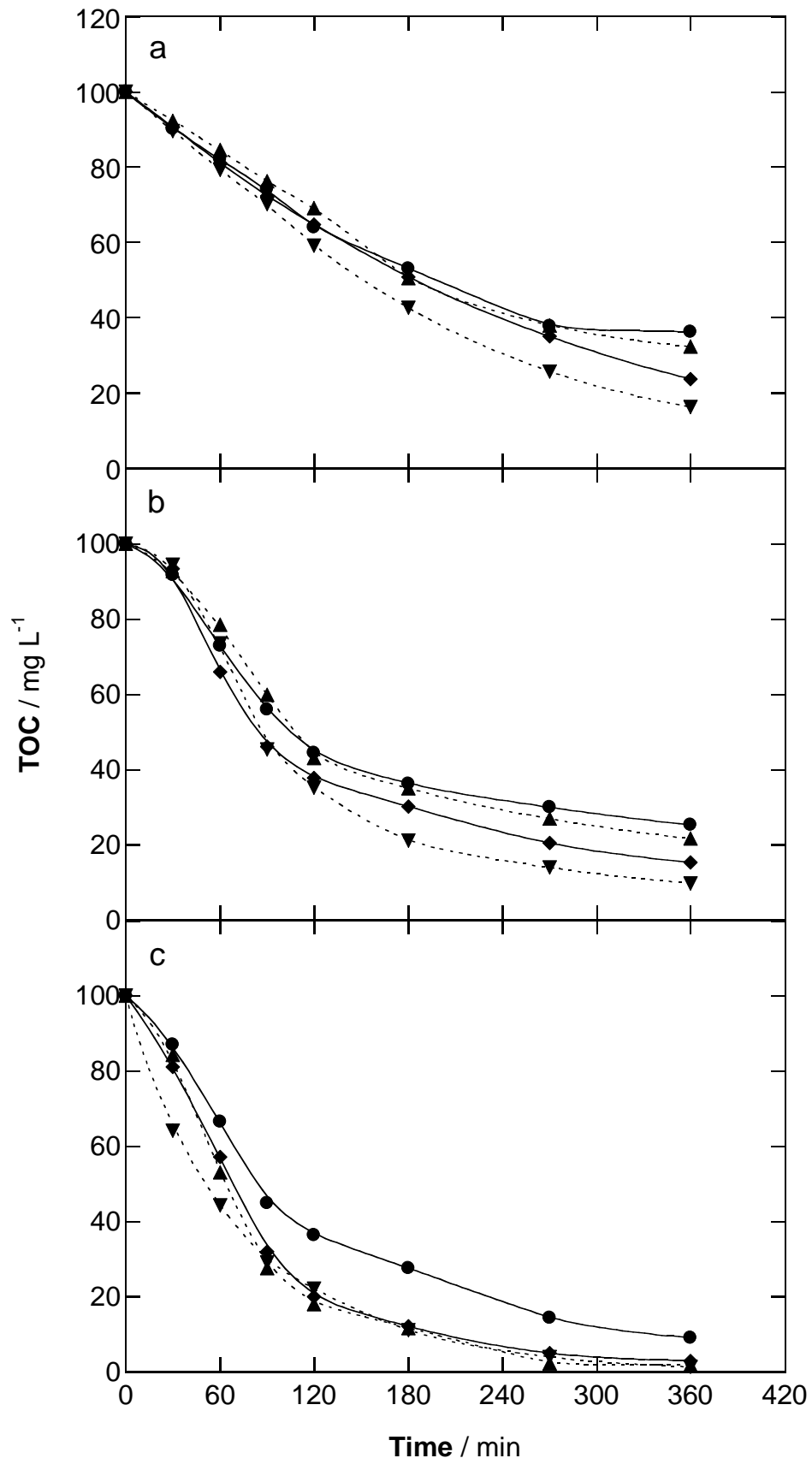


Fig. 3

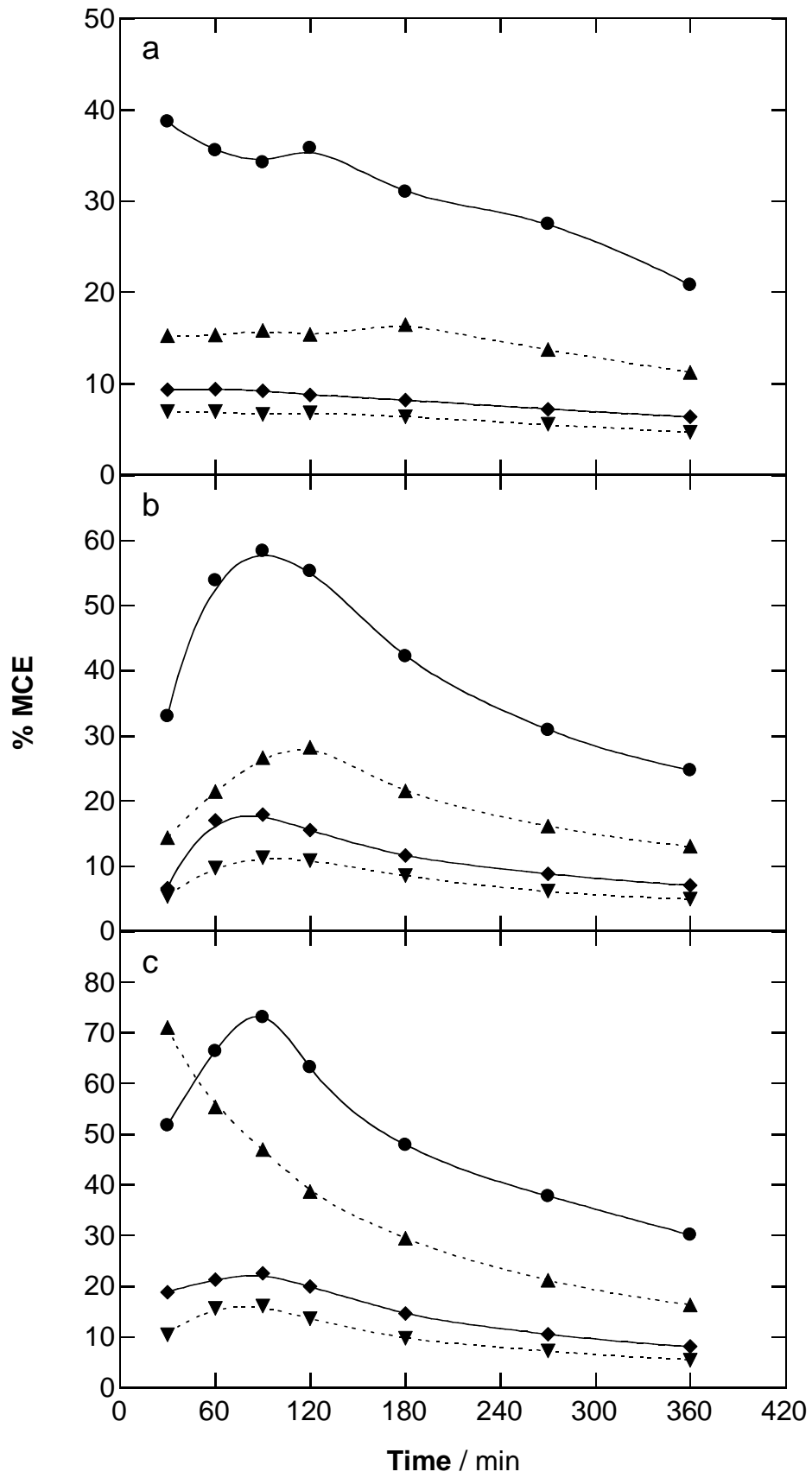


Fig. 4

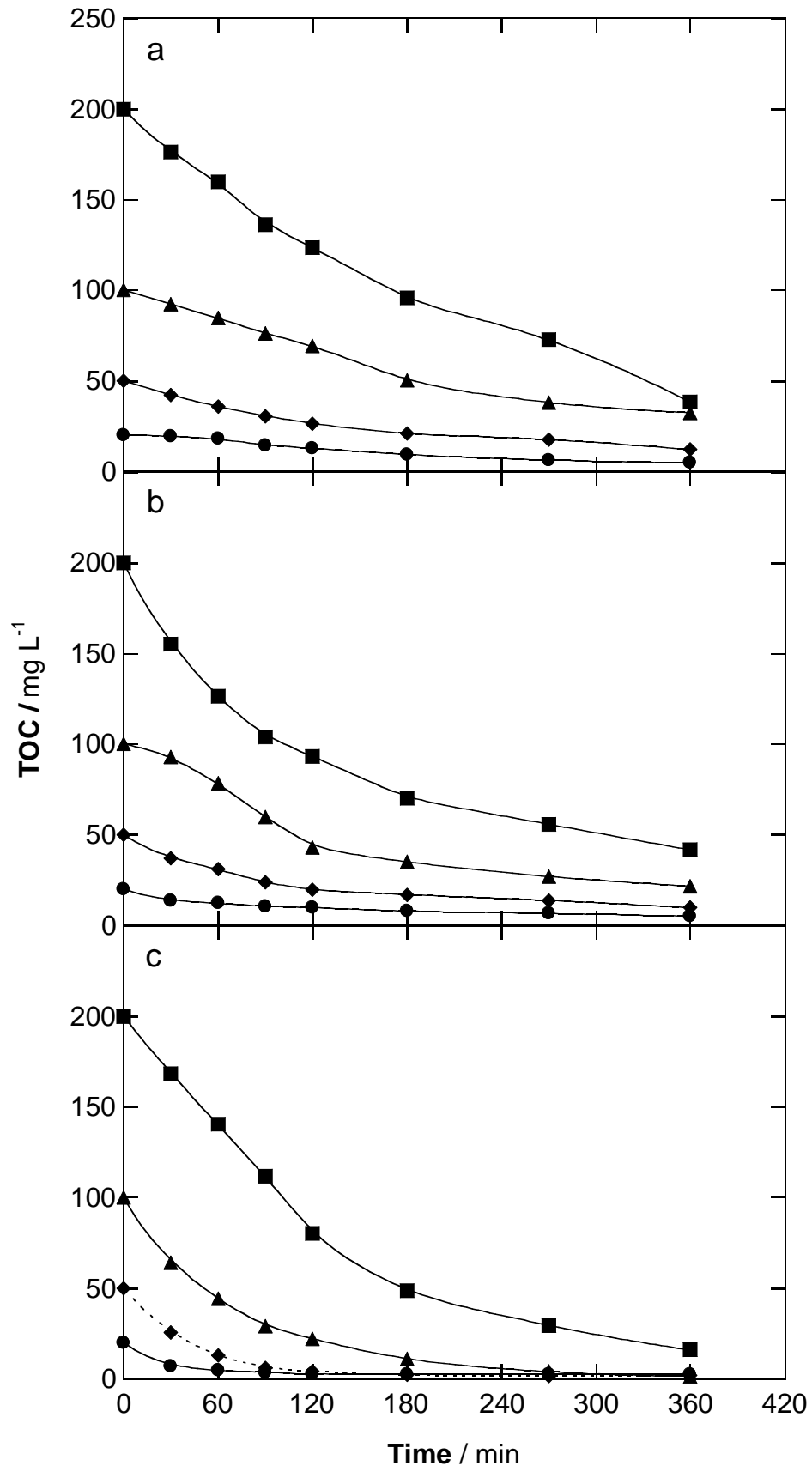


Fig. 5

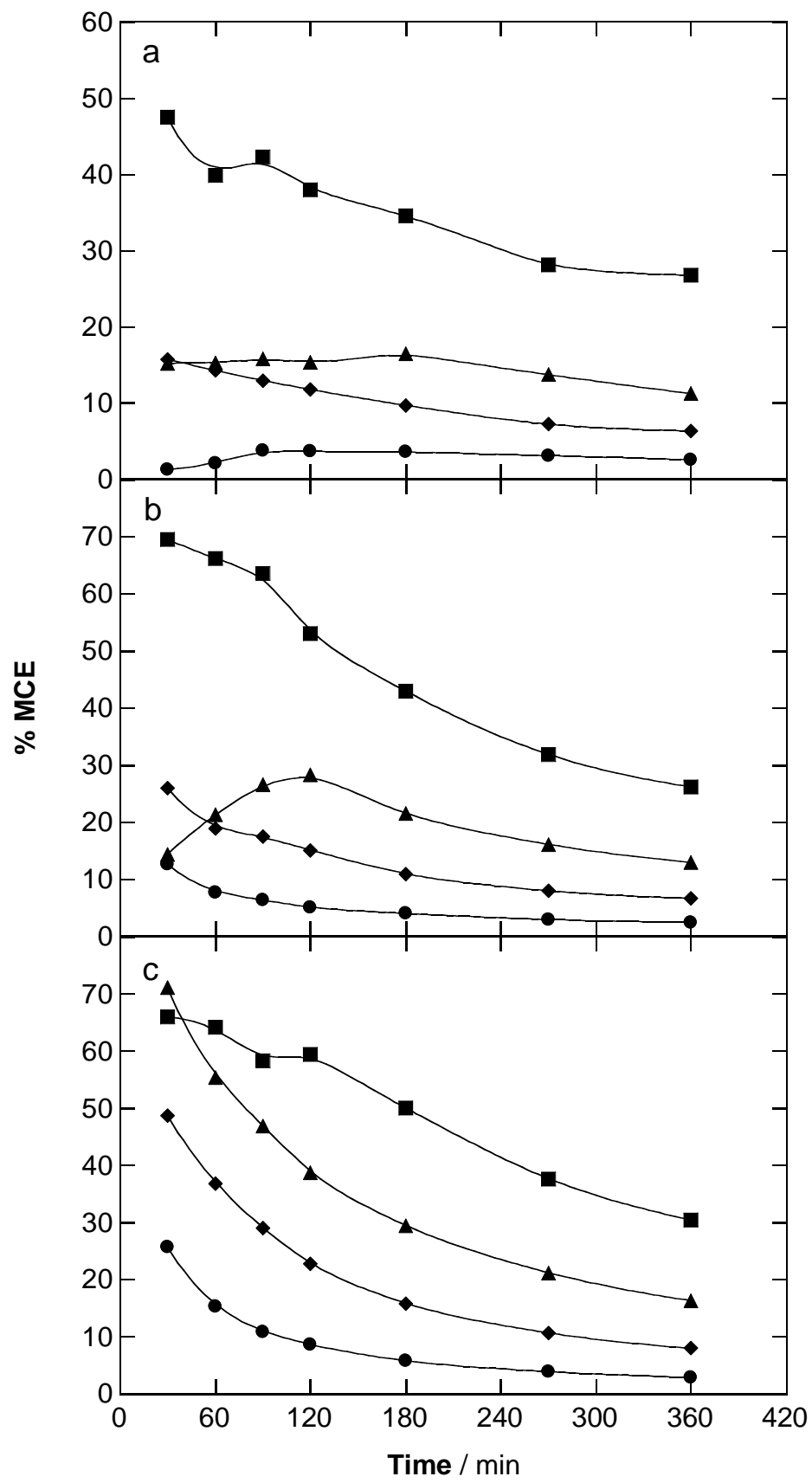


Fig. 6

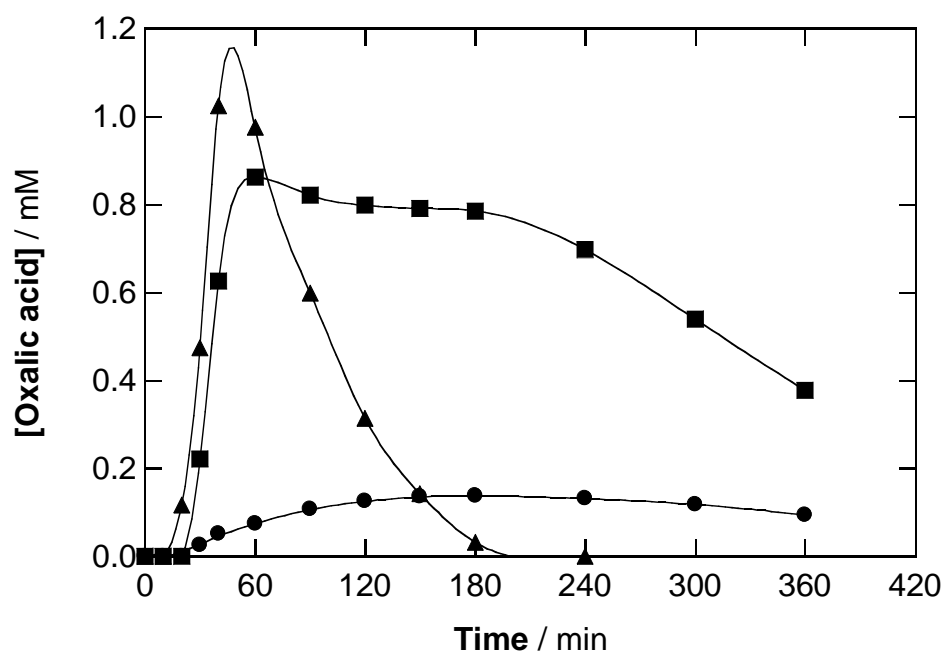


Fig. 7



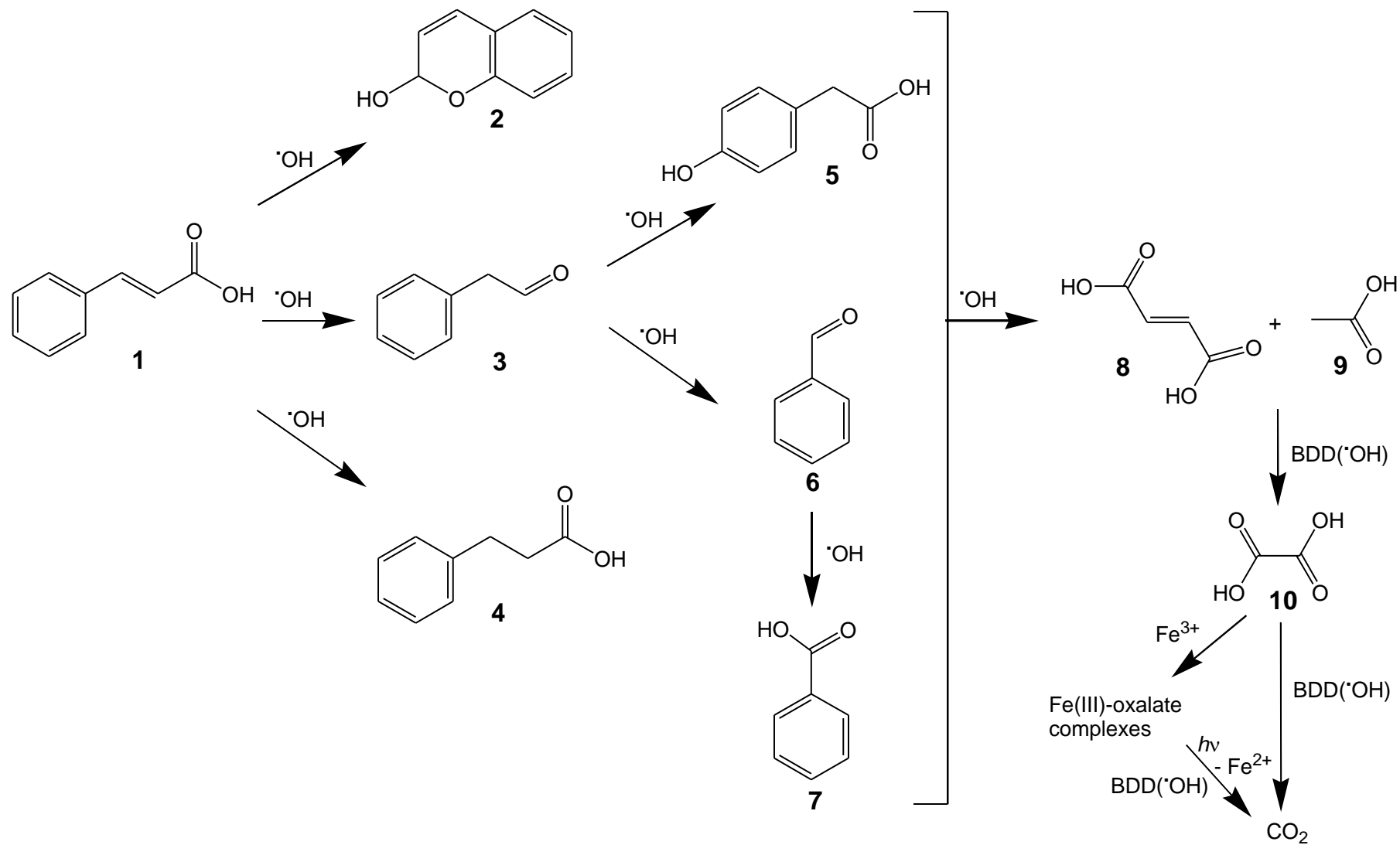
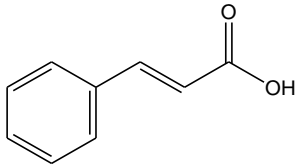
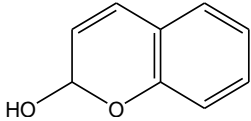
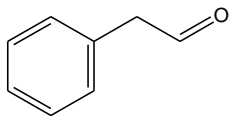
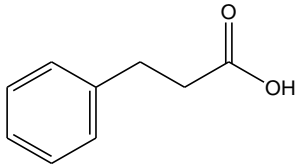
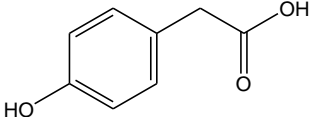
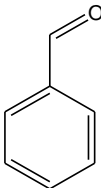
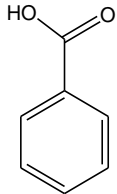


Fig. 8

**Table 1** Products identified by GC-MS during the electrolysis of 100 mL of a 0.926 mM *trans*-cinnamic acid solution in 0.05 M Na<sub>2</sub>SO<sub>4</sub> at pH 3.0 and 25 °C by AO-H<sub>2</sub>O<sub>2</sub> using a stirred BDD/air-diffusion cell at 33.3 mA cm<sup>-2</sup>.

Number	Name	Molecular structure	<i>t<sub>r</sub></i> (min)	<i>m/z</i>	Electrolysis time (min)
<b>1</b>	<i>trans</i> -Cinnamic acid		26.2 <sup>a</sup>	148 (M <sup>+</sup> ),	30, 90
			42.2 <sup>b</sup>	147, 131, 103	30, 90
<b>2</b>	2 <i>H</i> -1-Benzopyran-2-one or Coumarin		35.7 <sup>b</sup>	146 (M <sup>+</sup> ), 118, 90, 63	30, 90
<b>3</b>	Benzeneacetaldehyde		19.9 <sup>b</sup>	120 (M <sup>+</sup> ), 91, 65	30, 90
<b>4</b>	3-Phenylpropanoic acid		20.5 <sup>a</sup>	150 (M <sup>+</sup> ),	30, 90
			31.3 <sup>b</sup>	135, 107, 77	30, 90
<b>5</b>	4-Hydroxyphenylacetic acid		37.5 <sup>b</sup>	152 (M <sup>+</sup> ), 151, 137, 123, 109, 81	30, 90
<b>6</b>	Benzaldehyde		17.1 <sup>b</sup>	106 (M <sup>+</sup> ), 105, 77	30
<b>7</b>	Benzoic acid		35.3 <sup>b</sup>	122 (M <sup>+</sup> ), 105, 77, 51	30, 90
<b>10</b>	Oxalic acid	COOH-COOH	24.9 <sup>b</sup>	89 ((M-H) <sup>-</sup> ), 71, 50	90

Retention times for: <sup>a</sup> non-polar Agilent J&W HP-5ms and <sup>b</sup> polar HP INNOWax columns.